Supplementary information

Solution-shearing strategy for improved anchoring of self-assembled monolayers in inverted perovskite solar cells

Wenjun Xu, Lin Zhang, Jinghang Tang, Ying Yang*[a]

Experimental section

Materials

ITO (1.5 cm × 1.5 cm, 7 Ω sq^{-1}), PbI_2 (99.999%), MACl (99.99%), C_{60} (99.9%), NiO_x nanoparticle powder, [4-(3,6-dimethyl-9H-carbazol-9-yl)butyl] phosphonic acid (Me-4PACz), (2-(3,6-dimethoxy-9H-carbazol-9-yl)ethyl)phosphonic acid (MeO-2PACz), [4-(3,6-Diphenyl-9*H*-carbazol-9-yl)butyl]phosphonic acid (Ph-4PACz) and BCP (99%) were purchased from Advanced Election Technology Company in China. The solvents, including dimethylformamide (DMF), dimethyl sulfoxide (DMSO), isopropanol (IPA) and chlorobenzene (CB) were purchased from J&K (China) and used as received. Piperazine hydroiodide (PI) was purchased from Xi'an Yuri Solar. All materials were used directly without further purification.

Fabrication of Small-area Devices

Glass/ITO substrates (15 Ω sq-1) were sequentially cleaned by sonication with detergent, deionized water, acetone, and anhydrous ethanol for 15 min, respectively. Then, the glass/ITO substrates were dried at 100 °C in an oven, and then were treated with UV ozone for 15 min. Then the NiO_x solution (10 mg mL^{-1} in deionized water) was spin-coated on substrate at 3000 rpm for 20 s, followed by annealing in air at 110 °C for 10 mins. The NiO_x film was transferred to a N_2 glovebox. Three separate SAM solutions were prepared in isopropanol (IPA): Me-4PACz at 0.5 mg mL^{-1}, MeO-2PACz at 0.3 mg mL^{-1}, and Ph-4PACz at 0.3 mg mL^{-1}.For the spin-coated SAM devices, the SAM solution was deposited by either static spin coating (SSC) or dynamic spin coating (DSC) at 4000 rpm for 30 s, followed by annealing at 100 °C for 5 min. In SSC, the SAM solution was dispensed onto the stationary substrate before the spin-coating program was started. In DSC, the substrate was first accelerated to the target rotation speed, and the Me-4PACz solution was then dispensed onto the rotating substrate. For the blade-coated SAM devices, the SAM solution was deposited by either static blade coating (SBC) or dynamic blade coating (DBC). In SBC, the solution was first dispensed onto the substrate and then spread by blade coating. In DBC, the SAM solution was dispensed onto the substrate at the moment when blade movement was initiated. The blade-coating parameters were a coating speed of 5 mm s^{-1} and a blade gap of 100 μm, followed by annealing at 100 °C for 10 min.

For perovskite films, $Cs_{0.05}FA_{0.95}PbI_3$ solution with 1.5 M concentration was prepared by stoichiometrically mixing $CsPbI_3$ and $FAPbI_3$ a 4:1 (v/v) DMF:DMSO

solvent mixture. Additives of 7 mol% excess PbI_2 and 30 mol% MACl were incorporated into the precursor to enhance crystallization. The perovskite precursor (50 μL) was spin-coated at 4000 rpm for 20 s with an acceleration of 2000 rpm s^{-1}. 150 μL of CB was dropped onto the film at 8 s before the end of the spin-coating process, followed by immediate annealing at 150 °C for 30 mins. After cooling, the PI (1 mg mL^{-1} in IPA) was dynamic spin-coated at 5000 rpm for 30 s onto the perovskite layer, and annealing at 100 °C for 10 mins. C60 was then evaporated as the electron transport layer at a rate of 0.015 nm/s, followed by evaporation of BCP as a hole blocking layer at 0.01 nm/s. Finally, 100 nm Ag was evaporated as the electrode at a rate of 0.1 nm/s.

Sample characterization

UV-Vis: The absorption spectra of the films were characterized using a UV-Visible spectrophotometer (UV-1800, Shimadzu, Japan) within a scanning range of 300 to 1100 nm.

XRD: The crystalline phase of the films was analyzed using an X-ray diffractometer (SmartLab SE, Rigaku, Japan) with a 2θ scanning range of 10° to 50°. A scanning electron microscope (SEM) (JSM-IT700HR, Rigaku, Japan) was employed to characterize the surface morphology and microstructure of the films.

PL: The photoluminescence spectra of the films were tested using a fully functional fluorescence spectrometer (FLS1000, Edinburgh, UK) with an excitation wavelength of 405 nm.

XPS: X-ray photoelectron spectroscopy (XPS) (PHIVersaProbe 4, ULVAC-PHI, Japan) was used to characterize the elemental state of the perovskite film surfaces.

Photocurrent measurement: The current-voltage (J-V) characteristics of the perovskite solar cells (PSCs) were evaluated using a solar simulator (SS-F5-AAA, Enlitech, China) calibrated to AM1.5G with an intensity of 100 mW/cm^2 . The measurements were performed using test software (TIS-KA6000, Enlitech, China) over a scanning range of -0.1 to 1.3 V, with a step size of 50 mV and a scanning rate of 100 mV/s. The stabilized power output (SPO) and photocurrent were tested at the maximum power point of *J–V* plots of the PSC. The external quantum efficiency (EQE) spectra were obtained by a quantum efficiency measurement system (QE-R, Enlitech, Taiwan of China).

Durability measurement: A white LED lamp without UV filters (calibrated to AM1.5G) was used for operational stability test. All the small devices were tested under open-circuit (OC) conditions and without encapsulation.

Supplementary Note 1: Strain calculation by XRD**.**

Strain calculation through Williamson-Hall spots[1]: The broadening of the XRD peaks (β) is consisting of crystal size-induced broadening (β_D) and strain-induced broadening (βε), which is defined as:

$$\beta = \beta_D + \beta_\varepsilon$$

The crystal size-induced broadening (β_D) is defined through the Scherer equation:

$$D = \frac{K_\lambda}{\beta_D \cos\theta}$$

where D is the crystal size, K is the Scherer constant (~0.9 for perovskite), λ is the wavelength of X-ray (1.5418 Å), and 2θ is the XRD peak location. The strain-induced broadening (β_ε) is defined as:

$$\beta_\varepsilon = 4\varepsilon \tan\theta$$

Substituting Equation (2) and Equation (3) into Equation (1).

$$\beta \cos\theta = \varepsilon(4 \sin\theta) + \frac{K_\lambda}{D}$$

Supplementary Note 2: Fill factor (FF) loss analysis.

According to the S-Q limit theory, non-radiative recombination losses and charge transport losses cause the measured FF to be lower than the theoretical value[2]. General, the lower the non-radiative recombination loss of the device, the higher its maximum FF (FF_{max}) value. The FF_{max} can be calculated using the following equation:

$$FF_{max} = \frac{v_{OC} - ln(v_{OC} + 0.72)}{v_{OC} + 1}$$

The v_{OC} can be obtained by the following equation:

$$v_{OC} = \frac{V_{OC}}{nK_BT/q}$$

where n is the ideality factor extracted from the slope of the V_{OC}-light dependence curve. K_B is Boltzmann constant, and T is the temperature (300 K).

Supplementary Note 3:Urbach energy calculation

The slope of absorption edge from ultraviolet-visible (UV–vis) absorption spectra show an exponential relation with the Urbach energy (E_U), as described by the equation[3]:

$$\alpha = \alpha_0 e^{h_{v/E_U}}$$

where α is the absorption coefficient, hv is the photon energy and E_U is the Urbach energy.

Supporting figures and tables

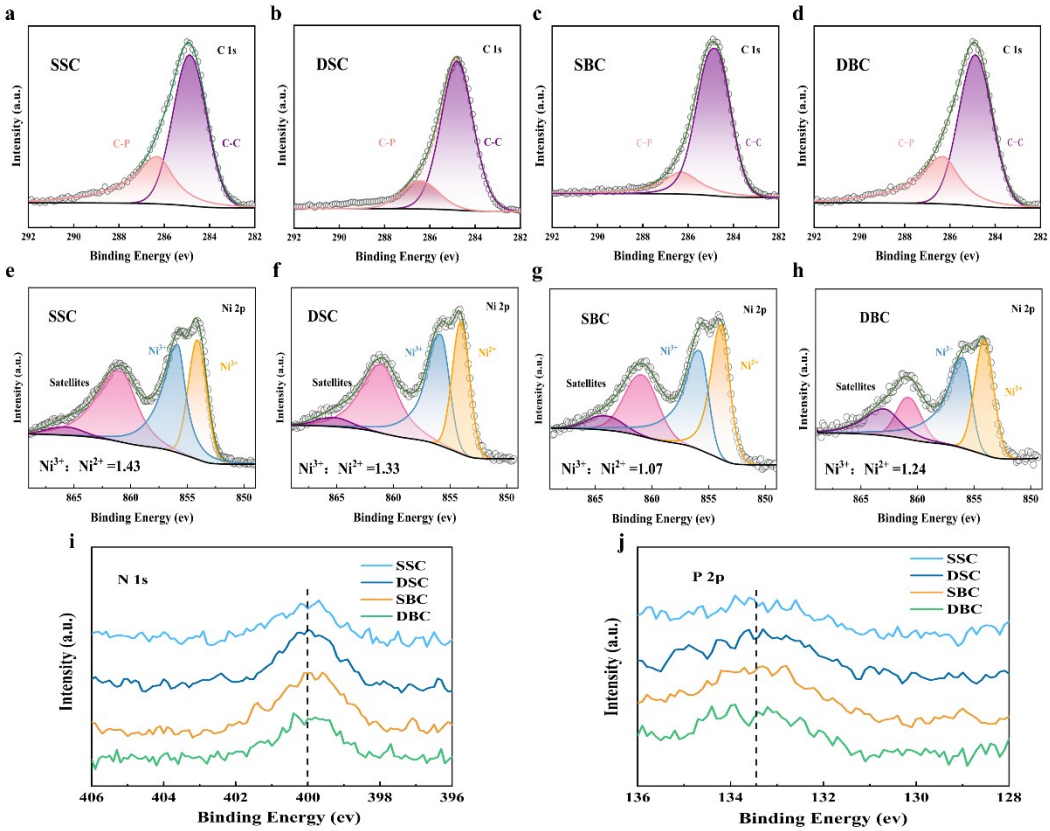

Figure S1. XPS characterization of HTLs. High-resolution XPS spectra of (a-d) C 1s, (e-h) Ni 2p ,(i) N 1s and (j) P 2p for films of NiO_x /Me-4PACz. Both SSC,DSC,SBC and DBC exhibit Ni^{2+}, Ni^{3+}, and satellite peaks in the Ni 2p spectra. Ni^{2+} primarily resides within the lattice, whereas Ni^{3+} is predominantly localized at the grain boundaries of non-stoichiometric oxygen-rich NiO_x. When Ni3+ directly interacts with organic cations in the perovskite, it may trigger redox reactions, leading to the deprotonation of organic cations and subsequent perovskite degradation. Through fitting of the Ni 2p XPS spectra and quantitative analysis of the peak area ratios, the Ni^{3+}/ Ni^{2+} ratios were determined to range from 1.33 to 1.43 for the spin-coated films and from 1.04 to 1.24 for the blade-coated films. This significant reduction in Ni^{3+} demonstrates effective passivation of NiO_x surface defects, which simultaneously accelerates interfacial charge transport and improves device operational stability.

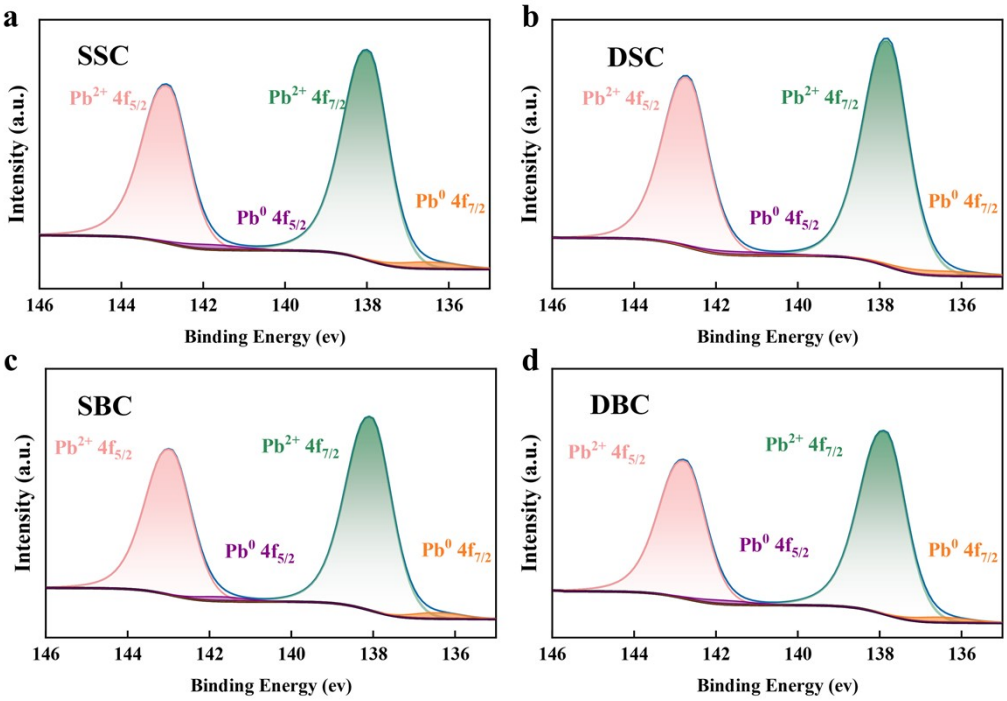

Figure S2. Pb 4f XPS spectra of the buried interface of fresh perovskite films.

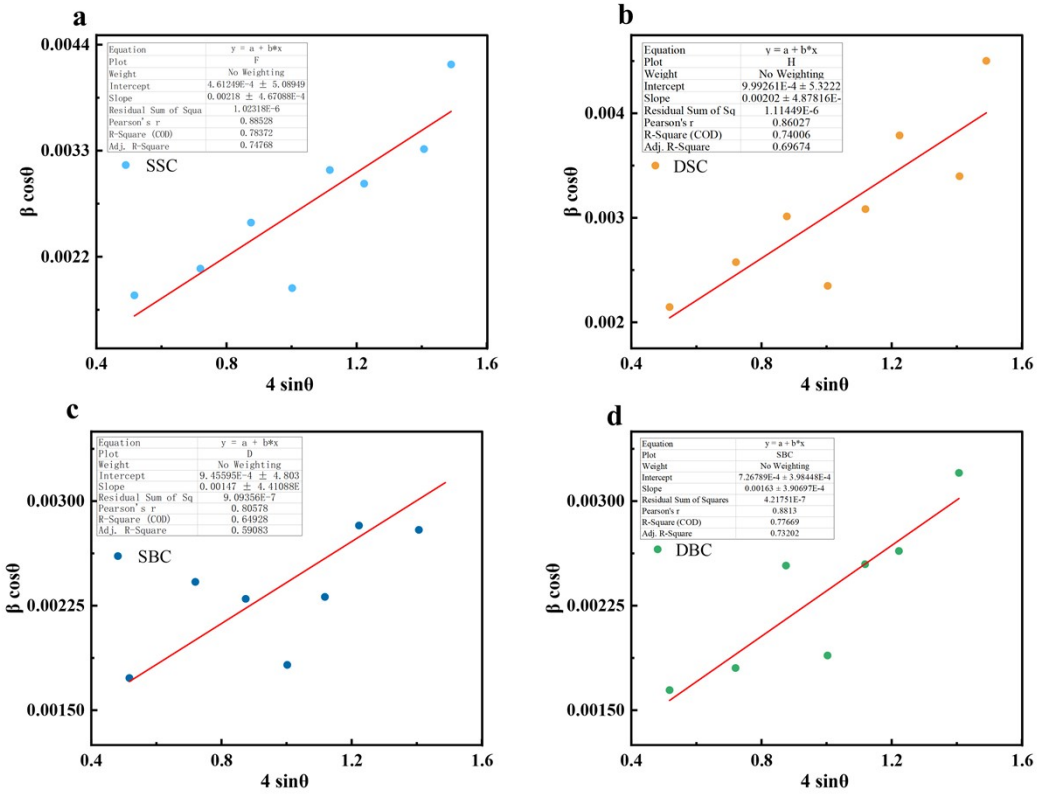

Figure S3. (a-d) Williamson−Hall plots in PVKs.

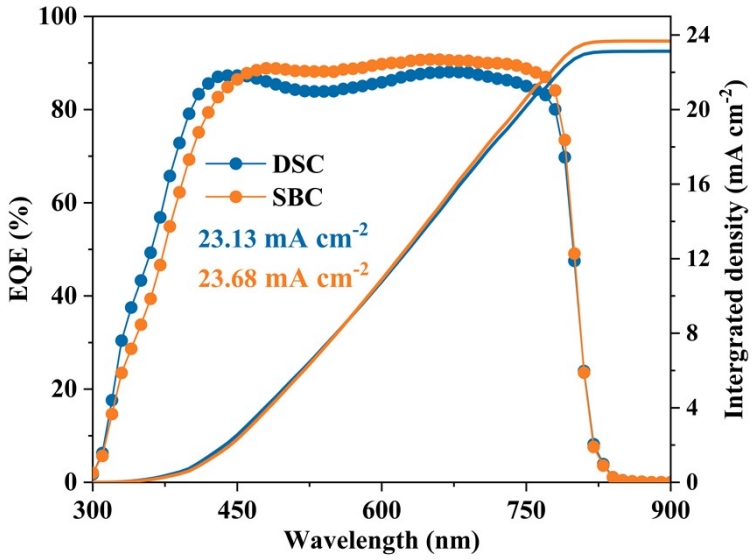

Figure S4. EQE spectra with the integrated J_{SC} of the DSC and SBC devices.

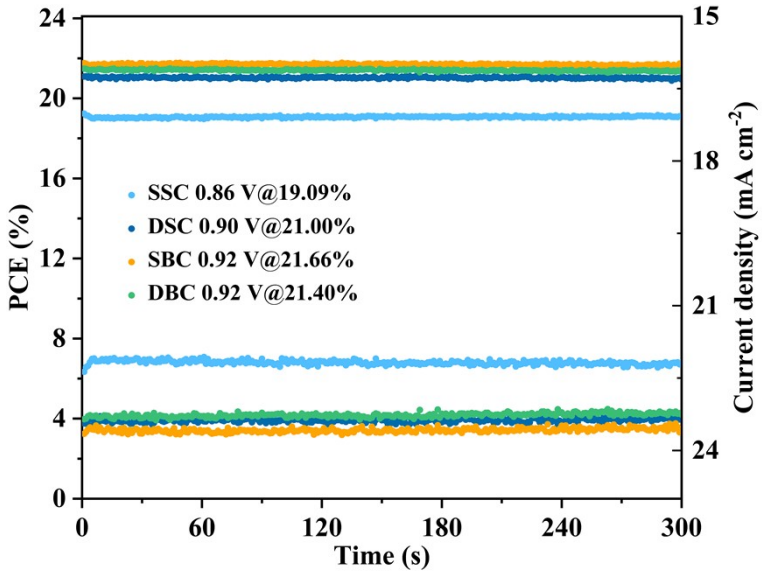

Figure S5. Time-dependent stabilized power output measurements measured at maximum power points of the PSCs.

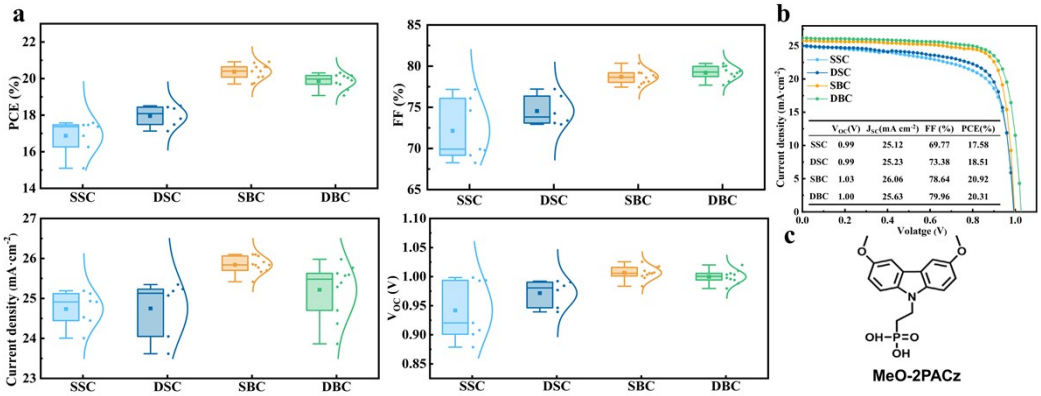

Figure S6. (a) Distribution of PCE, V_{OC}, FF, and J_{SC} of SSC, DSC, SBC and DBC devices based on Meo-2PACz. (b). J–V curves of the champion devices. (c) Molecular structures of MeO-2PACz.

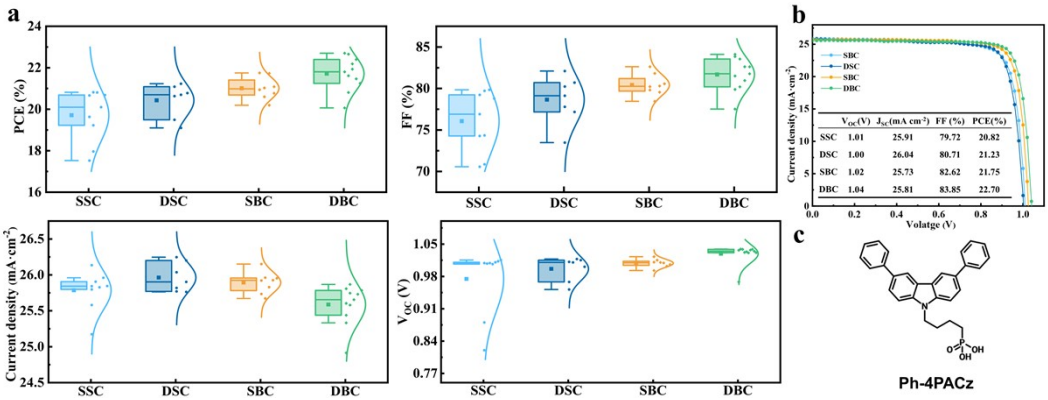

Figure S7. (a) Distribution of PCE, V_{OC}, FF, and J_{SC} of SSC, DSC, SBC and DBC devices based on Meo-2PACz. (b). J–V curves of the champion devices. (c) Molecular structures of Ph-4PACz.

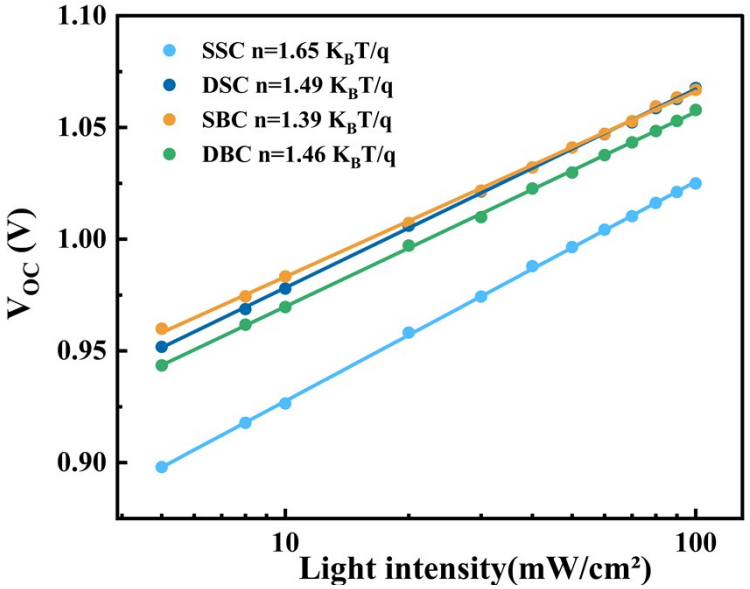

Figure S8. Illumination intensity dependent Voc of SSC,DSC,SBC and DSC devices.

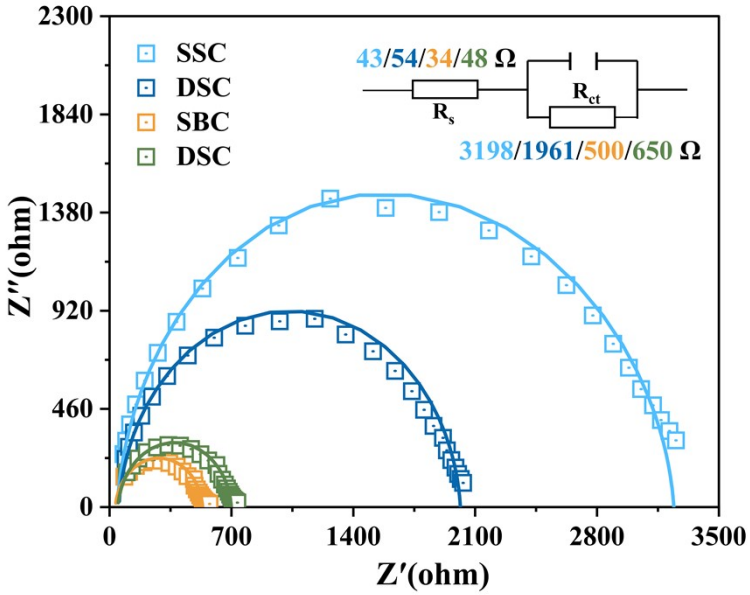

Figure S9. (e) EIS curves of SSC,DSC,SBC and DSC devices under the dark conditions. The inset is its fitting circuit.

Table S1. The proportion of each element atom ratio of high-resolution XPS spectra for NiO_x/SAMs.

Sample	C atm%	N atm%	P atm%	Ni atm%
SSC	**62.12**	**3.25**	**2.79**	**31.83**
DSC	**67.64**	**3.65**	**3.97**	**24.75**
SBC	**78.16**	**4.63**	**4.47**	**12.74**
DBC	**75.55**	**3.45**	**4.02**	**16.97**

Table S2. The proportion of each element atom ratio of high-resolution XPS spectra for perovskite films at the buried interface.

Sample	C atm%	Pb atm%	I atm%
SSC	**90**	**3.89**	**6.11**
DSC	**93.39**	**4.01**	**2.59**
SBC	**83.89**	**4.31**	**11.8**
DBC	**90.56**	**2.65**	**6.79**

References

1. X. Chen, M. Yang, X. Sun, X. Li, Y. Xie, X. Feng, J. Tang, L. Yan, S. Fan and S. Dai, Acs Energy Lett, 2025, 10, 3620-3628.
2. Z. Lv, Z. Wang, G. Liu, Y. Gao, S. Li, Z. Liu, M. Xu, J. Cheng, W. Zhao and W. Lu, Adv. Mater., 2026, 38, e13600.
3. Q. Yin, T. Chen, J. Xie, R. Lin, J. Liang, H. Wang, Y. Luo, S. Zhou, H. Li and Z. Wang, Adv. Mater., 2024, 36, 2405840.